Ultrasoft microgels displaying emergent, platelet-like, behaviors

Supplementary Materials:

Materials and Methods:

Phage biopanning assays

Biopanning assays were performed with a phagemid libraries that display variable domain-like recognition motifs (sdFv)[1]. The stock phage library was produced in a non-suppressor *E. coli* strain (TG1) and purified with polyethylene glycol according to the previously established protocol from Lee *et al* [2]. For biopanning assays, fibrin clots were formed *in vitro* by combining purified human fibrinogen, thrombin, and factor XIII at physiologically relevant concentrations (2 mg/mL); fibrin was allowed to polymerize for 1hr prior to initiating biopanning assays. Clots were blocked with 5% powdered milk in phosphate buffer (137 mM NaCl, 2.7 mM KCl, 10 mM Na_2HPO_4, 2 mM KH_2PO_4; pH 7.4; MPBS). The purified phage library (5 x 10^{12} phage particles) was then incubated with fibrin clots allowing the phage to bind to the target. After removal of the supernatant, the fibrin clots were subjected to a series of rinses with PBS + 0.1% Tween 20 (PBST) to rid the surface of non-specific binding phage. Next, a solution of soluble fibrinogen was overlaid on top of the fibrin clot to remove phage that recognize soluble fibrinogen and thereby increase the specificity of the fibrin-binding phage. The fibrin bound phage were then eluted from the fibrin clot, collected, and amplified. Subsequent rounds were repeated with an enriched population of eluted phage from the previous round. Outcome measurements after each round of screens included titers of initial phage stock, rinse solution, and eluted phage. After three rounds of binding selections, 96

clones for each library were selected and grown to produce phage and soluble sdFv according to the previously established protocol [2]. Identical screens were performed with the Tomlinson I and J libraries, which display human derived single chain variable fragment antibody (scFv) containing both the heavy chain variable region (V_H) and the light chain kappa variable region of human IgG [1].

Enzyme-Linked Immunosorbent Assay (ELISA)

Fibrin specificity was evaluated via enzyme-linked immunosorbent assay (ELISA). Soluble sdFv fragments possess a myc-tag, thus enabling binding detection via biotinylated anti-myc monoclonal in conjunction with streptavidin-HRP. Both fibrin and fibrinogen ELISAs were performed to identify clones with preferential binding affinity to fibrin over fibrinogen. Thin layers of fibrin were formed in the 96-well plates via layer-by-layer deposition of fibrinogen-thrombin-fibrinogen [3]. Separate fibrinogen-coated 96-well plates were prepared to run parallel ELISAs with the same scFv or sdFv clones. Each ELISA plate also contained positive controls (i.e. ubiquitin coated wells with clones specific to ubiquitin) and negative controls (i.e. random clones and non-antigen coated wells). Plates were blocked with 2% MPBS for 2 h at room temperature (RT). Freshly prepared scFv/sdFv supernatant was then incubated for 1 h at RT. Plates were thoroughly rinsed with PBST prior to incubation with diluted anti-myc biotin (Sigma Aldrich; 1:2000) for 1hr at RT. Plates were again thoroughly rinsed with PBST prior to incubation with Extravidin-HRP conjugate (Sigma Aldrich; 1:1000) for 1hr at RT. HRP was developed using 1-Step Ultra-TMB-ELISA solution for ~15min (Thermo Scientific); the reaction was stopped using 2 N sulfuric acid and absorbance was quantified with a spectrophotometer (Molecular Devices; 450nm).

Production of sdFvs

Select phage clones that demonstrated preferential binding affinity to fibrin were used to infect a non-suppressor *E. coli* strain (HB2151) to produce the soluble sdFv without the pIII fusion motif. HB2151 cells were grown at 37 °C and sdFv expression was induced with IPTG. Following induction, cells were grown at 28 °C for 20 h. The supernatant was collected, filtered and sdFv was then purified using protein A affinity chromatography (AKTA Purifier, GE Healthcare, Piscataway, NJ, USA).

SPR

Based on previous SPR protocols developed in our lab [4], a thin fibrin layer was immobilized on the surface of a gold SPR chip via layer-by-layer deposition of fibrinogen-thrombin-fibrinogen [3]. SdFvs were flowed across the fibrin surface and the binding interactions were evaluated and recorded. Additionally, sdFv binding interactions with a surface of immobilized fibrinogen was used to investigate the specificity to fibrin. All SPR data was examined and analyzed with Scrubber 2 and Clamp XP (Center for Biomolecular Interactions Analysis, University of Utah). Data simulation curves were generated based on a Langmuir 1:1 binding model assuming only a single ligand-analyte interaction.

SdFv-microgel synthesis and characterization

Ultralow cross-linked (ULC) microgels (μgels) with highly deformable, dendritic architecture were prepared using standard seeded precipitation polymerization techniques previously described [5]. A 95%pNIPAm/5%AAc composition (poly(*N*-isopropylacrylamide-*co*-acrylic acid) was utilized for microgel synthesis, which results in microscaffolds ~1μm diameter in the swollen state. Co-polymerization with acrylic acid

was utilized to allow for carboxylic acid chemoligation sites for sdFv attachment [6,7]. Following synthesis, μgels were purified using ultracentrifugation and conjugated to fibrin specific sdFvs using standard EDC/NHS chemistry. For confocal fluorescence microscopy experiments, sdFvs were also labeled with maleimide-Alexa Fluor-488 following conjugation to the μgels. To determine basic μgels properties, the particles were characterized using dynamic light scattering to determine the hydrodynamic radius and atomic force microscopy imaging to characterize morphology. Finally, to ensure that μgels coupled to fibrin-specific sdFvs retained fibrin-binding capabilities, binding of sdFv-μgels to fibrin was determined through interferometry analysis utilizing the Fortébio Blitz system. Similarly as described for SPR analysis, for interferometery analysis, a thin fibrin layer was immobilized onto an amine reactive sensor chip (Ar2G, Fortébio).

Clot polymerization/degradation assays

Thrombin-initiated fibrin polymerization and degradation assays were used to evaluate clotting rates and persistence in the presence of H6 or S11 (control) ULC μgels. Competing polymerization and degradation reactions were created with a 96 well plate, and a final volume of 100 μL per well. Two solutions were made, a fibrinogen-μgel solution that was loaded initially, and a thrombin-tPA (tissue Plasminogen Activator)-plasminogen solution that was added in a 1:1 volume ratio. Final concentrations in each well were 2 mg/mL μgel and 2 mg/mL of fibrinogen, 5 mM $CaCl_2$, 0.25 U/mL of human thrombin (Enzyme Research Laboratories, Inc., South Bend, IN), 0.29 μg/mL of tissue plasminogen activator (tPA), and 10.8 μg/mL of plasminogen. Reactions were performed in a 25 mM Hepes, 150 mM NaCl buffer. Turbidity curves were generated from

absorbance measurements (SpectraMax M2 Microplate Reader, Molecular Devices, Sunnyvale, CA) at 350 nm, with reads taken every thirty seconds.

Dynamic in vitro clotting assays

To characterize the effect of μgels on clotting *in vitro*, we utilized an endothelialized microfluidic device that recapitulates the cellular, physical, and hemodynamic environment of microcirculation, similarly to a device previously described[8]. Endothelial cells are cultured inside of the device to prevent non-specific protein binding over the device channels. Moreover, the endothelialized device creates an *in vivo* like assay, which is more physiologically relevant than a bare device (without endothelial cells). The human vessel wall is composed of endothelial cells which themselves respond to critical clotting factors, like thrombin and others, and directly contribute to pro-clotting and anti-clotting processes. In order to more accurately mimic the dynamic interplay between blood plasma proteins, microvascular endothelial cells, and platelets, it is necessary to use a system that attempts to recapitulate these critical features. The microfluidic device is controlled by a syringe pump that generates continuous flow (PHD syringe pump, Harvard Apparatus). The microfluidic device is comprised of three regions of different flow rates, comprising four endothelialized channels. The designed and calculated shear rates are 1, 10 and 100 s^{-1} for the four left-most channels, the four right-most channels and the four center channels, respectively. Shear rates are calculated without endothelial cells. The thickness of endothelial cell is negligible to affect the shear rate in our device, so we assume the shear rates of the device are identical regardless of the existence of endothelial cells.

The polydimethylsiloxane (PDMS) device was fabricated using a conventional photolithography and soft lithography process. To prepare the photomask for a SU-8 mold, AutoCAD was used to design the microfluidic channel, and the designed patterns were transferred onto the chrome mask for further processing. SU-8 2050 was spin coated over the silicon wafer at 3000 rpm for 30 sec, which results in a 50 μm thick photoresist film. UV light was exposed over the film through the patterned chrome mask followed by development process using a SU-8 developer. The patterned SU-8 mold was silanized using hexamethyldisilazane (HMDS) in order to prevent it from adhering to the cured PDMS. 10:1 (elastomer:curing agent) mixed PDMS mixture (SYLGARD 184, Dow Corning) was poured over the SU-8 mold and cured at 65 °C overnight. The cured PDMS was peeled off from the SU-8 mold and holes were punched for the inlet and outlet. And the punched PDMS device was covalently bonded to a thin PDMS membrane by oxygen plasma treatment.

In preparation for cell seeding, fibronectin (50 μg/ml) from human plasma (Sigma-Aldrich) was injected into the microfluidic channels to coat the inside walls, and the device was incubated at 37 °C, 5 % CO_2 for 1 hour. Cells (HUVEC) were prepared and concentrated to 10×10^6 cells/ml in cell culture media (EGM-2, Lonza) with 8% mass/volume dextran (Sigma-Aldrich). Then, the prepared cells were pipette injected into the microfluidic channels and incubated in the cell culture incubator for 1 hour. Afterward, fresh cell culture media (EGM-2) was perfused through the device for 2 days at a flow rate of 1.5 μl/min using a syringe pump.

Following 2 days in culture, dynamic clotting assays were performed. For these experiments, clotting of platelet poor plasma (PPP) was analyzed in the absence or

presence of fibrin-binding μgels of varying degrees of crosslinking in real time using confocal microscopy. As a control, clotting of platelet rich plasma (PRP) or PPP in the presence of non-fibrin binding μgels was also investigated. μgels or buffer were added to PPP immediately prior to injection into the microfluidic device. To visualize clotting, all plasma samples were spiked with Alexa Fluor-488 labeled fibrinogen. Endothelial cells were stained with Cell Mask Deep Red (Invitrogen) and μgels were labeled with Alexa Fluor 546. For experiments utilizing PRP, platelets were stained with Cell Mask Red (Invitrogen). Samples were flowed at 1.1 μL/min and imaged continuously for 20 min. To simulate conditions of massive hemorrhaging, experiments were also performed in which PLPs were added to PPP diluted 1:1 with saline. To examine the utility of PLPs for augmentation of clotting in additional coagulopathies, experiments were performed in which PLPs were added to PPP collected from neonatal patients following complex cardiac surgery requiring cardiopulmonary bypass, a condition which is known to induce dilutional coagulopathy leading to bleeding complications[9,10], or to PPP collected from hemophiliac patients which have a FVIII/FIX deficiency which inhibits fibrin protofibril formation.

Clot collapse analysis

Fibrin clot structure was analyzed using confocal microscopy. Fibrin clots with and without sdFv-μgels were prepared using 2 mg/mL fibrinogen and 0.25 U/mL thrombin and examined using confocal microscopy (Zeiss 510 VIS). To allow for visualization of the μgels and fibrin matrix, Alexa Fluor 647-labeled fibrinogen and Alexa Fluor 488 or 546-labeled μgels were utilized for these assays. Clots were formed directly on a glass slide, overlaid with a coverslip and allowed to polymerize for an hour prior to imaging [11-

[13]. Clots were also imaged 24 hours post polymerization to monitor changes in clot structure over time. Macroscopic clot deformation was analyzed through gross clot collapse assays. Clots were formed in silinized glass tubes from PPP through the addition of 1 U/mL human α-thrombin (Enzyme Research Laboratories). H6- μgels with varying degrees of crosslinking or S11-ULC μgels were added to the clots prior to addition of thrombin.

Clot Collapse Simulations

We use dissipative particle dynamics (DPD) [14-16] to examine the dynamic response of fibrin network on incusing on soft and stiff particles. DPD is a coarse-grained simulation technique that employs a momentum-conserving thermostat and soft repulsive interactions among beads representing clusters of molecules. This allows tackling physical phenomena that occur at relatively large time and spatial scales [17-20].

In DPD, the time evolution of the many-body system obeys Newton's second law $m d\mathbf{v}_i/dt = \mathbf{f}_i$, where $\mathbf{v}_i$ and $\mathbf{f}_i$ are, respectively, the velocity and force on bead i with mass m, and t is time. The equations of motion are integrated using the velocity-Verlet algorithm [14]. The force on a bead is $\mathbf{f}_i = \sum_j \left(\mathbf{F}_{ij}^C + \mathbf{F}_{ij}^D + \mathbf{F}_{ij}^R\right)$, where the sum runs over all beads j within a cutoff radius r_c around bead i. The conservative force is given by $\mathbf{F}_{ij}^C = a_{ij}\left(1-\hat{r}_{ij}\right)\hat{\mathbf{r}}_{ij}$, where a_{ij} is the repulsion between beads i and j, $\hat{r}_{ij} = r_{ij}/r_c$ and $\hat{\mathbf{r}}_{ij} = \mathbf{r}_{ij}/r_{ij}$, with $r_{ij} = \left|\mathbf{r}_i - \mathbf{r}_j\right|$. The dissipative force is $\mathbf{F}_{ij}^D = -\gamma\,\omega^D\left(r_{ij}\right)\left(\hat{\mathbf{r}}_{ij}\cdot\mathbf{v}_{ij}\right)\hat{\mathbf{r}}_{ij}$ and the random force is $\mathbf{F}_{ij}^R = \sigma\,\omega^R\,\xi_{ij}\hat{\mathbf{r}}_{ij}\sqrt{dt}$, where $\mathbf{v}_{ij} = \mathbf{v}_i - \mathbf{v}_j$ and ξ_{ij} is a zero-mean Gaussian random variable of unit variance with $\xi_{ij} = \xi_{ji}$. The coefficients γ and $\sigma^2 = 2k_BT\gamma$ determine the strength of dissipative and random forces, where k_B is the Boltzmann

constant and T is the temperature of the system. The weight functions ω^D and $\omega^R = 1 - \hat{r}_{ij}$ are related via $\omega^D = \left(\omega^R\right)^2$. This relation and the strength of dissipative and random forces are set to ensure thermodynamic equilibrium [16]. We set the time step $\Delta t = 0.01$, $m = 1$, $r_c = 1$, $\gamma = 4.5$, $a = 25$, $k_B T = 1$ and the solvent number density $\rho = 3$ (all dimensional values are given in DPD units).

The fibrin network is modeled using a random network of elastic filaments [21,22]. Such networks capture the mechanical properties of disordered polymer networks [23]. The flexible filaments are formed from nodes connected by harmonic springs with a spring constant $k_f = 300$ and an equilibrium length $r_{eq} = 0.5$, and bending springs with a bending stiffness $k_b = 50$. To build a random network, we distribute crosslink points with a number density 0.01 and then connect them by filaments with average connectivity equal to 4. The initial network has a spherical shape with the outer diameter equal to 50. The network interacts with the DPD solvent via DPD potentials.

Stiff particles are formed by clustering DPD beads on an FCC lattice with fixed inter-particle distances. The particles composed of 80 beads and are characterized by the Stokes-Einstein radius of about 0.9. Soft particles are composed of 9 polymer chains attached together to form a star-like macromolecule. Each chain consists of 10 DPD beads connected by harmonic springs with properties identical to those of the fibrin network. The radius of gyration of soft particles is about 0.9. To mimic attraction between particles and fibrin network, we use a Morse potential. The equilibrium distance of the potential is set to 0.7, whereas the potential strength ε is varied to probe the effect of particle adhesiveness on network collapse.

We conduct our simulations in a square periodical box with sides equal to 55.

Simulations were conducted in a stagnant fluid to mimic experimental conditions. At the beginning of the simulations, we randomly distribute 20 particles inside initially spherical fibrin network and then continue the simulations until a new steady state is reached. To characterize changes taking place in fibrin network, we measure the network radius of gyration.

Femoral Vessel Injury Model:

To test the efficacy of PLPs in hemostasis, we utilized a well-established rat femoral vessel traumatic injury model [24-26]. This model results in an easily visualized, continuous stream of blood flowing from the injury site. All protocols were approved by the Georgia Institute of Technology IACUC. Adult Sprague-Dawley male rats (200-250 g) were anesthetized with 5% isoflurane. Following anesthesia, an incision was made on the right hindlimb to expose the femoral vessels. A portion of the femoral vein was isolated from the surrounding connective tissue by placing a small piece of foil between the vessel and the underlying tissue. Following isolation of the vessel, the cavity was irrigated with 0.9% irrigation fluid at 37 °C. Animals were then administered 500 μL of saline (vehicle), purified human factor VIIa (hFVIIa, 100 μg/kg the current standard of care, purchased from Innovative Research), PLPs (20 mg/mL), S11-ULC μgels (20 mg/mL) via tail vein injection using a 24 gauge catheter. Six animals were tested per condition. Following a 5 minute circulation time, injury was induced to the right femoral vein by piercing the vein with a 22 gauge needle. A gauze was lightly placed below the injury site to collect blood, allowing for better visualization of the injury site as well as measurement of total blood loss. Gauze were changed every ten seconds for the first 30 seconds following injury and then every 30 s until bleeding ceased. Bleeding time was

defined as the time required for bleeding to cease for a minimum of 10 s. To compare reduction of bleeding times due to PLPs to that of natural platelets, in a separate experiment, we also evaluated bleeding times following a 500 μL injection of freshly isolated rodent platelet rich plasma or saline. The protocol utilized for isolation of rodent PRP results in ~$1X10^9$ platelets/ml similar to previously reported values[27]. This concentration is similar to the typical concentration range of platelets transfused clinically[28]. This is compared to the 20 mg/mL of PLPs infused, which corresponds to ~ $1X10^7$ particles/mL. This concentration of PLPs was chosen based on pilot studies that indicated this dose decreased bleeding times compared to control groups. Bleeding times are expressed as percent reduction compared to saline injections to allow for comparisons between experiments (Fig S8). Following cessation of bleeding, animals were euthanized with carbon dioxide and organs separated, fixed with 10% formalin, paraffin embedded and 5 μm sections were produced using a Microm 355H Microtome (Thermo Scientific). Co-localization of PLPs were characterized through immunofluorescence staining for the myc-tag encoded on the sdFvs and through Martius Scarlet Blue (MSB) staining for fibrin in adjacent serial sections. For myc-tag staining, samples were counter stained with Hoescht (Invitrogen) to visualize nuclei.

Statistical Analysis

All statistical analyses for bleeding time studies were performed with Prism software program (GraphPad, San Diego CA). Bleeding and blood weight data were statistically analyzed using repeated measures analysis of variance using the Tukey test at a 95% confidence interval.

Supplemental Figures

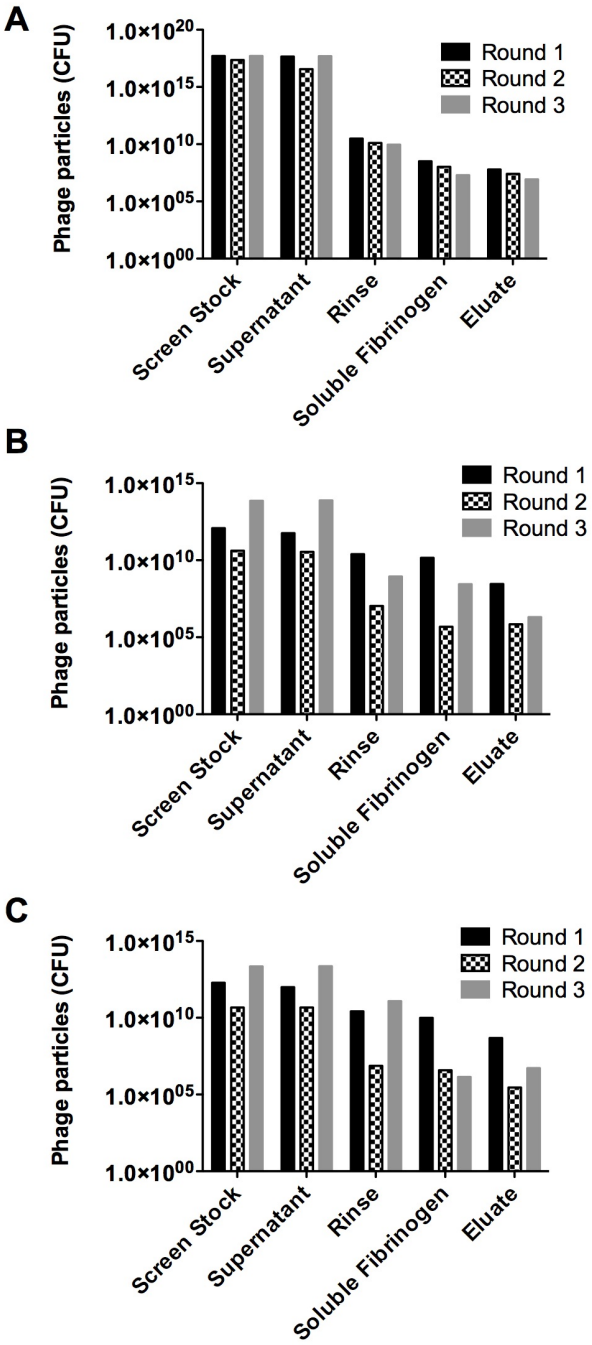

Figure S1: *Biopanning assays: All libraries titer.* Phage Titers for biopanning screens against fibrin clots for (A) sdFv library, (B) Tomlinson I library, and (C) Tomlinson J library. All biopanning screens were performed three times with increasing stringency in the rinse phase.

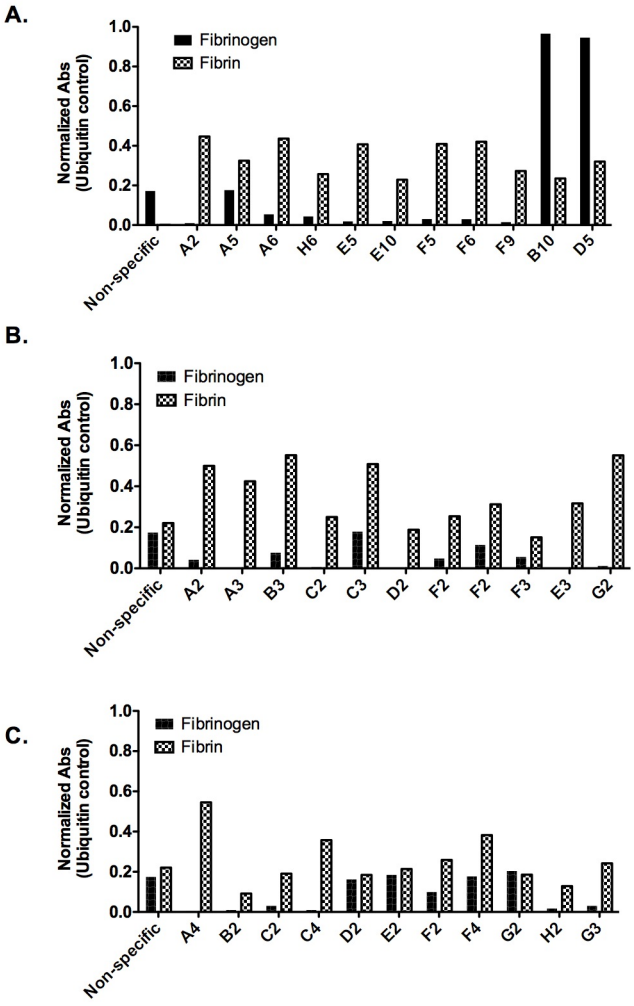

Figure S2: *Biopanning assays:* ELISA 10 clones all libraries. Representative fibrin and fibrinogen ELISA results for (A) sdFv library, (B) Tomlinson I library, and (C) Tomlinson J library. Absorbance results were normalized to positive ubiquitin control.

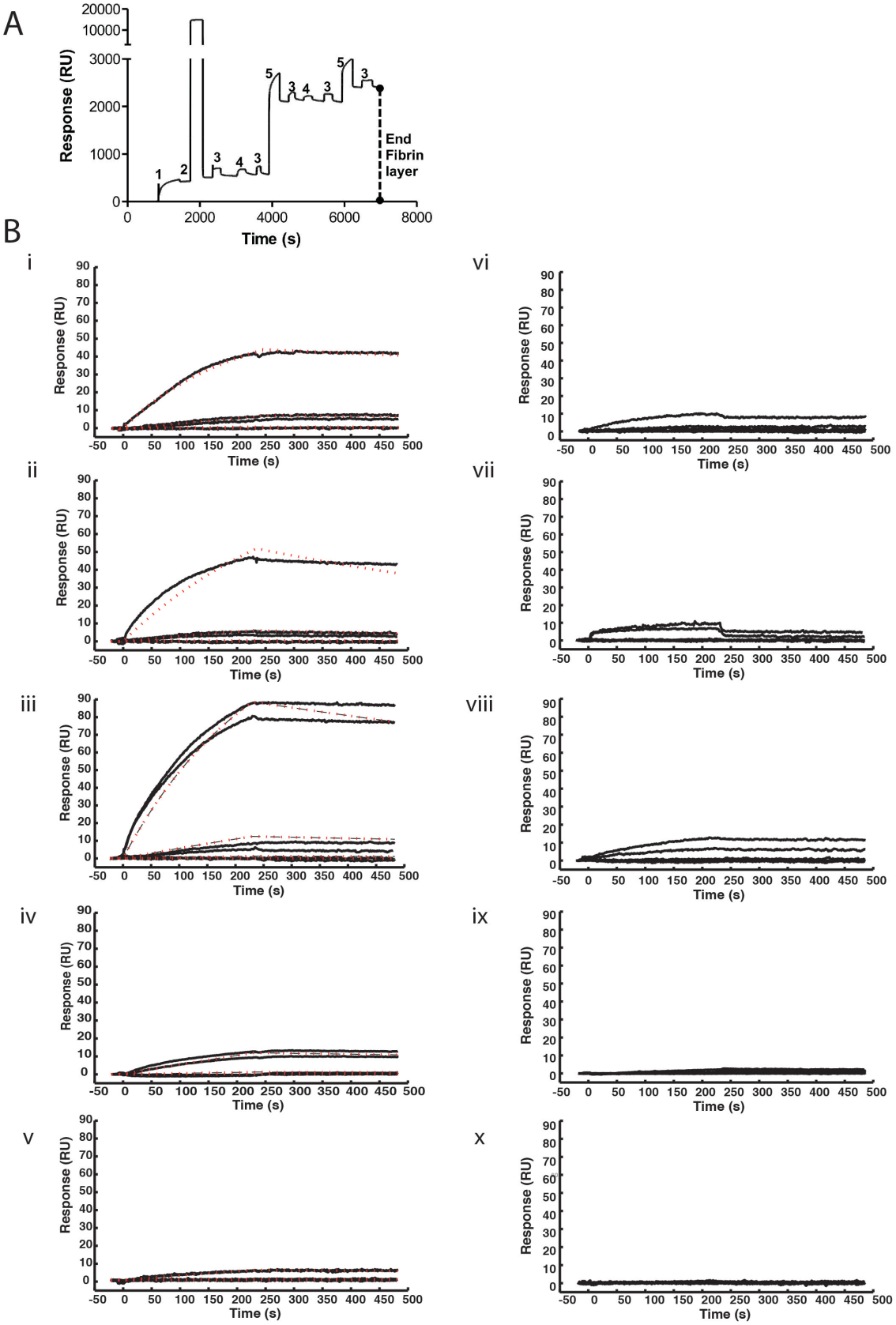
A
Response (RU)
Time (s)
End
Fibrin
layer
B
i
ii
iii
iv
v
vi
vii
viii
ix
x

Figure S3: *SPR analysis fibrin-binding sdFvs and scFvs:* (A) SPR sensorgram of thin fibrin layer immobilized on surface the SPR channel via NHS/EDC activated carboxylic acid terminated SAM with subsequent injections of fibrinogen (1), ethanolamine quencher (2), HEPES buffer + Tween 20 (3), thrombin (4), and fibrinogen+anti-thrombin+heparin (5). (B) Representative SPR sensorgrams of sdFvs on fibrin layer (i-v) or BSA surface (vi-x) for clones A2 (i, vi), A6 (ii, vii), H6 (iii, viii), B3 (iv, ix), or non-specific control (v, x). Experimental data is shown in black and fits are shown in red.

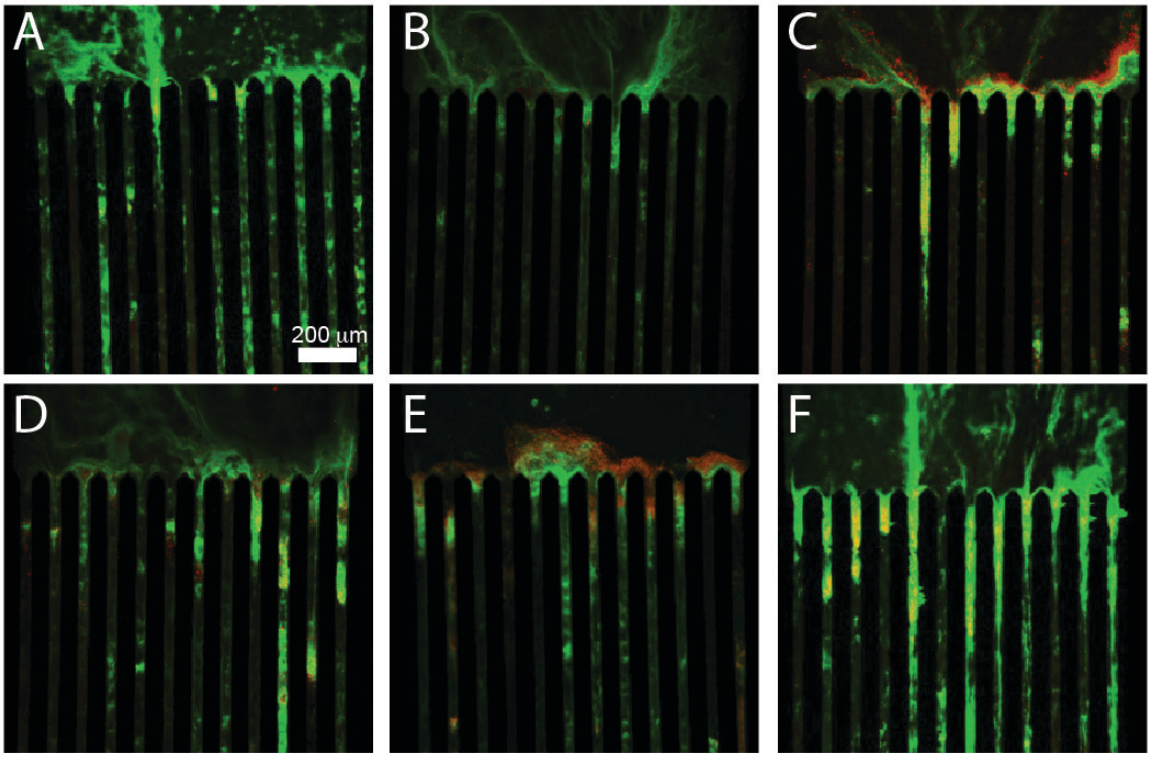

Figure S4: *Effect of particle deformability on in vitro clotting*. PLPs (A) H6-2% (B), H6-4% (C), H6-7% (D), H6-PS (E) and PRP (F). Fibrin=green; microgels=red

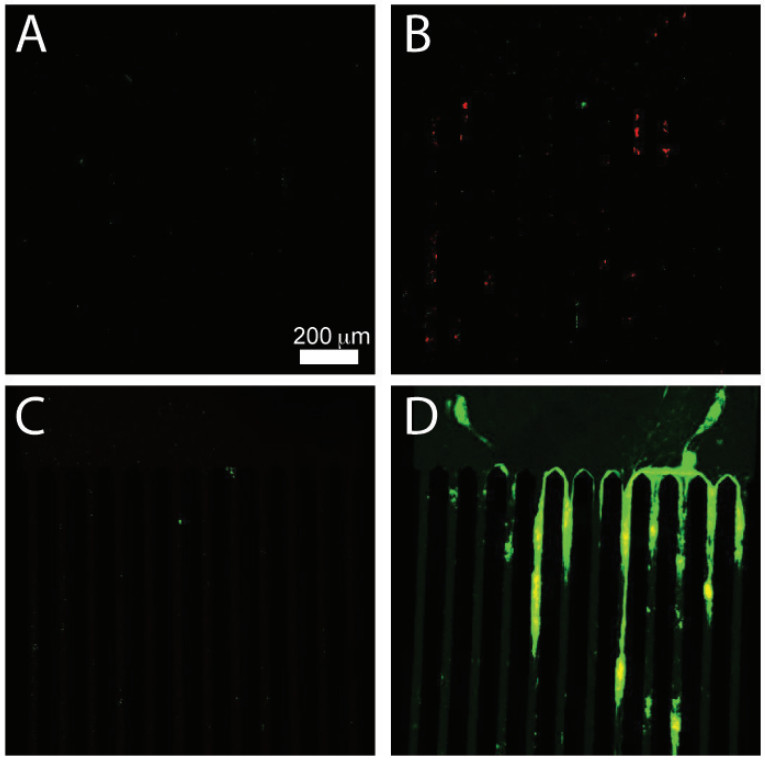

Figure S5: *Utility of PLPs in augmentation of clotting in compromised patient samples utilizing an endothelialized microfluidics device*. Clotting of PPP collected from a hemophiliac patient in the absence (A) or presence of PLPs (B). Clotting of PPP collected from a neonatal cardiac surgery patient following removal from cardiopulmonary bypass in the absence (C) or presence (D) of PLPs. Fibrin=green; microgels=red

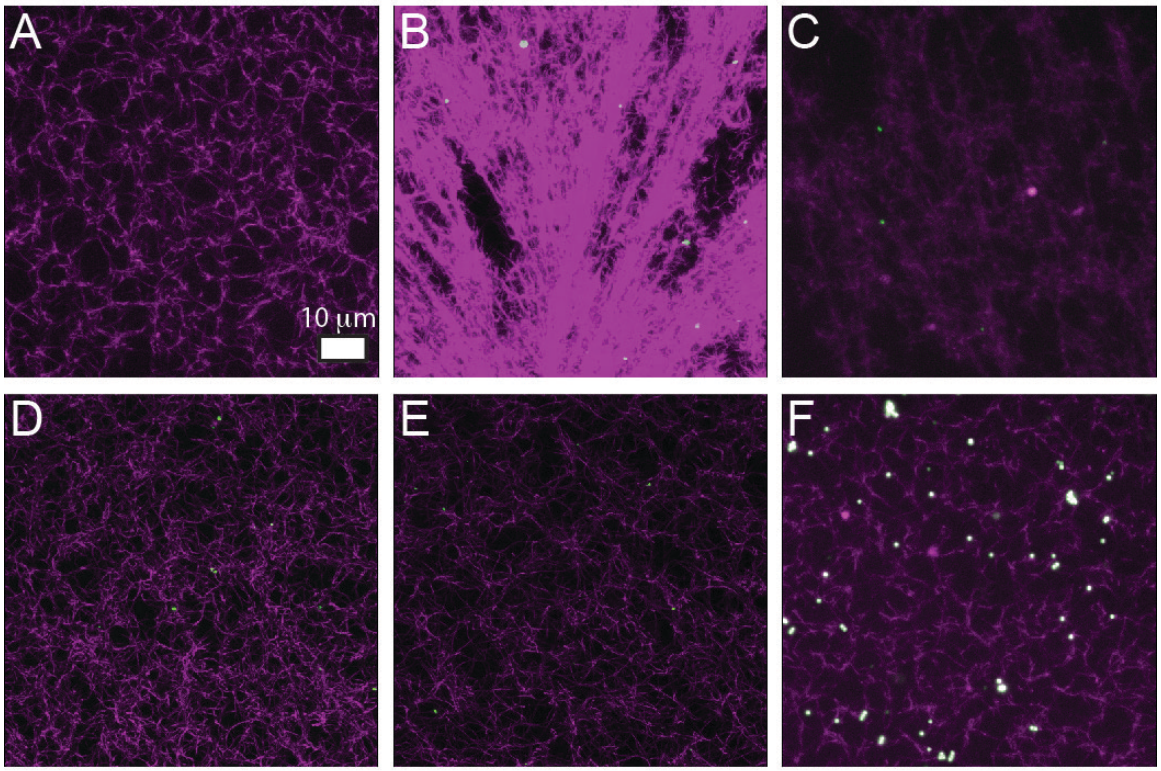

Figure S6: *Effect of particle deformability on microscopic clot structure.* Fibrin clots were formed in the absence or presence of H6-conjugated μgels from 2 mg/mL fibrinogen and 0.25 U/mL thrombin. 1 hour following polymerization, clots were analyzed via confocal microscopy. Fibrin only (A), H6-ULC μgels (PLPs) (B), H6-2% bis μgels (C), H6-4% bis μgels (D), H6-7% bis μgels (E) and H6-PS particles (F) were analyzed. Fibrin=magenta. microgels=green.

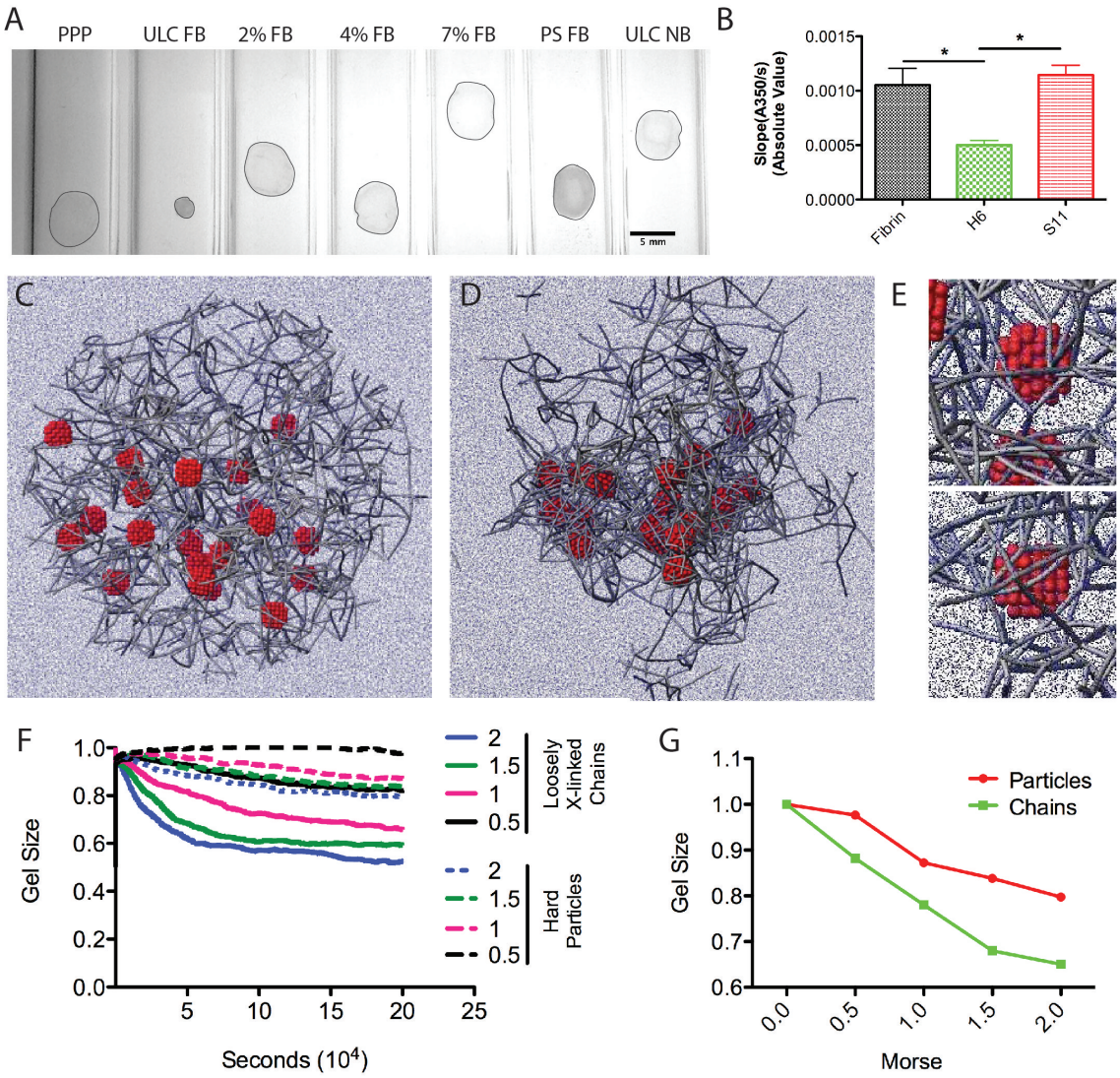

Figure S7: *Effect of particle deformability on macroscopic clot structure.* Clot collapse 48 hours post polymerization of clots formed from PPP in the presence or absence of fibrin binding (H6) μgels with various degrees of crosslinking or nonbinding (S11) ULC μgels (A). Clot degradation rates were characterized in absence or presence of fibrin-binding (H6) or non-binding S11-ULC μgels through endogenous fibrinolysis assays (B). Clot collapse simulation results with hard, binding particles embedded in fibrin network. The clot is shown at the beginning (C) and end (D) of the simulation. Increased magnification images of particles at various locations in the network are shown (E). The effect of particle attractiveness for the fibrin network on clot size over time (F) and final clot size (G) are shown for both hard particles and loosely cross-linked chains embedded within the fibrin network.

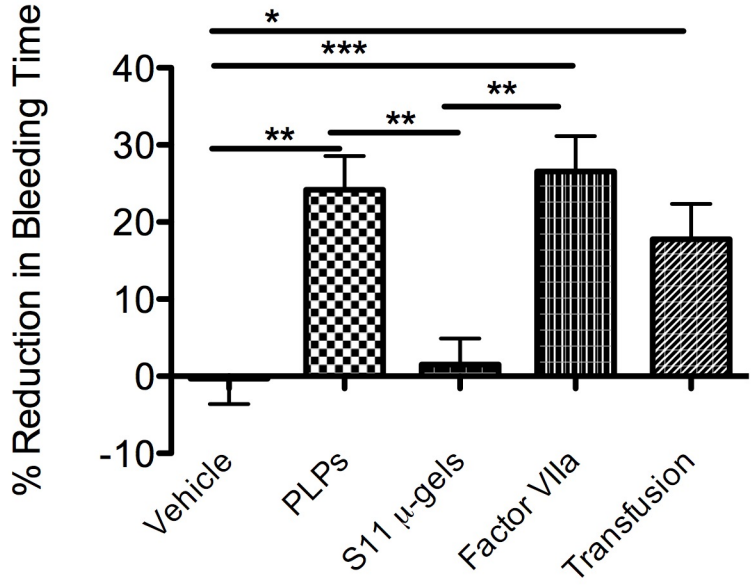

Figure S8: *Percent reduction in bleeding times in femoral vessel injury model.* Rats were administered saline (vehicle), PLPs, S11 μgels, Factor VIIa or transfusion of freshly isolated PRP and following a 5-minute circulation time, a femoral vein injury was induced. Percent reduction in bleeding times compared to vehicle only controls is presented.

Videos

Video 1: *Clotting PRP*

Video 2: *Clotting PPP*

Video 3: *Clotting PPP + Fibrin Binding Microgels*

Video 4: *Clotting PPP + Non-fibrin binding Microgels*

Video 5: *Clotting Diluted PPP + Fibrin Binding Microgels*

Video 6: *Clot collapse simulation with loosely cross-linked particles*

Video 7: *Clot collapse simulation with hard particles*

References

1 Lee, C. M., Iorno, N., Sierro, F. & Christ, D. Selection of human antibody fragments by phage display. *Nature protocols* **2**, 3001-3008, doi:10.1038/nprot.2007.448 (2007).

2 Lee, C. M., McGuire, H., Basten, A., King, C. & Christ, D. Expression, purification and characterization of recombinant interleukin-21. *Journal of immunological methods* **362**, 185-189, doi:10.1016/j.jim.2010.08.008 (2010).

3 Riedel, T., Brynda, E., Dyr, J. E. & Houska, M. Controlled preparation of thin fibrin films immobilized at solid surfaces. *Journal of biomedical materials research. Part A* **88**, 437-447, doi:10.1002/jbm.a.31755 (2009).
4 Stabenfeldt, S. E., Gossett, J. J. & Barker, T. H. Building better fibrin knob mimics: an investigation of synthetic fibrin knob peptide structures in solution and their dynamic binding with fibrinogen/fibrin holes. *Blood* **116**, 1352-1359, doi:10.1182/blood-2009-11-251801 (2010).
5 Jones, C., Lyon, LA. Synthesis and characterization of multiresponsive core-shell microgels. *Macromolecules* **33**, 8301-8306 (2000).
6 Blackburn, W. H., Dickerson, E. B., Smith, M. H., McDonald, J. F. & Lyon, L. A. Peptide-functionalized nanogels for targeted siRNA delivery. *Bioconjugate chemistry* **20**, 960-968, doi:10.1021/bc800547c (2009).
7 Dickerson, E. B. *et al.* Chemosensitization of cancer cells by siRNA using targeted nanogel delivery. *BMC cancer* **10**, 10, doi:10.1186/1471-2407-10-10 (2010).
8 Tsai, M. *et al.* In vitro modeling of the microvascular occlusion and thrombosis that occur in hematologic diseases using microfluidic technology. *The Journal of clinical investigation* **122**, 408-418, doi:10.1172/JCI58753 (2012).
9 Guzzetta, N. A., Amin, S. J., Tosone, A. K. & Miller, B. E. Change in heparin potency and effects on the activated clotting time in children undergoing cardiopulmonary bypass. *Anesthesia and analgesia* **115**, 921-924, doi:10.1213/ANE.0b013e318267056b (2012).
10 Guzzetta, N. A. *et al.* An evaluation of the effects of a standard heparin dose on thrombin inhibition during cardiopulmonary bypass in neonates. *Anesthesia and analgesia* **100**, 1276-1282, doi:10.1213/01.ANE.0000149590.59294.3A (2005).
11 Stabenfeldt, S. E., Gourley, M., Krishnan, L., Hoying, J. B. & Barker, T. H. Engineering fibrin polymers through engagement of alternative polymerization mechanisms. *Biomaterials* **33**, 535-544, doi:10.1016/j.biomaterials.2011.09.079 (2012).
12 Stabenfeldt, S. E., Aboujamous, N. M., Soon, A. S. & Barker, T. H. A new direction for anticoagulants: Inhibiting fibrin assembly with PEGylated fibrin knob mimics. *Biotechnology and bioengineering*, doi:10.1002/bit.23184 (2011).
13 Soon, A. S., Lee, C. S. & Barker, T. H. Modulation of fibrin matrix properties via knob:hole affinity interactions using peptide-PEG conjugates. *Biomaterials* **32**, 4406-4414, doi:10.1016/j.biomaterials.2011.02.050 (2011).
14 Groot, R. D. & Warren, P. B. Dissipative particle dynamics: Bridging the gap between atomistic and mesoscopic simulation. *J. Chem. Phys.* **107**, 4423-4435 (1997).
15 Hoogerbrugge, P. J. & Koelman, J. M. V. A. Simulating Microscopic Hydrodynamic Phenomena with Dissipative Particle Dynamics. *Europhys. Lett.* **19**, 155-160 (1992).
16 Espanol, P. & Warren, P. Statistical-Mechanics of Dissipative Particle Dynamics. *Europhys Lett* **30**, 191-196 (1995).
17 Groot, R. D. & Rabone, K. L. Mesoscopic simulation of cell membrane damage, morphology change and rupture by nonionic surfactants. *Biophys. J.* **81**, 725-736 (2001).

18 Chen, S., Phan-Thien, N., Fan, X. J. & Khoo, B. C. Dissipative particle dynamics simulation of polymer drops in a periodic shear flow. *J Non-Newton Fluid* **118**, 65-81, doi:DOI 10.1016/j.jnnfm.2004.02.006 (2004).

19 Fedosov, D. A., Karniadakis, G. E. & Caswell, B. Dissipative particle dynamics simulation of depletion layer and polymer migration in micro- and nanochannels for dilute polymer solutions. *Journal of Chemical Physics* **128**, 144903, doi:Artn 144903 Doi 10.1063/1.28971761 (2008).

20 Ripoll, M., Ernst, M. H. & Espanol, P. Large scale and mesoscopic hydrodynamics for dissipative particle dynamics. *J. Chem. Phys.* **115**, 7271-7284 (2001).

21 Masoud, H. & Alexeev, A. Modeling magnetic microcapsules that crawl in microchannels. *Soft Matter* **6**, 794-799, doi:Doi 10.1039/B916835d (2010).

22 Masoud, H. & Alexeev, A. Controlled Release of Nanoparticles and Macromolecules from Responsive Microgel Capsules. *Acs Nano* **6**, 212-219, doi:Doi 10.1021/Nn2043143 (2012).

23 Buxton, G. A. & Clarke, N. "Bending to stretching" transition in disordered networks. *Phys. Rev. Lett.* **98**, 238103, doi:Artn 238103 Doi 10.1103/Physrevlett.98.238103 (2007).

24 Bertram, J. P. *et al.* Intravenous hemostat: nanotechnology to halt bleeding. *Science translational medicine* **1**, 11ra22, doi:10.1126/scitranslmed.3000397 (2009).

25 Fuglsang, J. *et al.* Platelet activity and in vivo arterial thrombus formation in rats with mild hyperhomocysteinaemia. *Blood coagulation & fibrinolysis : an international journal in haemostasis and thrombosis* **13**, 683-689 (2002).

26 Ersoy, G. *et al.* Hemostatic effects of microporous polysaccharide hemosphere in a rat model with severe femoral artery bleeding. *Advances in therapy* **24**, 485-492 (2007).

27 Messora, M., Nagata, M., Furlaneto, F., Dornelles, R., Bomfim, S., Deliberador, T., Garcia, V., Bosco, A. A standardized research protocol for platelet-rich plasma (PRP) preparation in rats. *RSBO* **8**, 1806-7727 (2011).

28 Singh, R. P., Marwaha, N., Malhotra, P. & Dash, S. Quality assessment of platelet concentrates prepared by platelet rich plasma-platelet concentrate, buffy coat poor-platelet concentrate (BC-PC) and apheresis-PC methods. *Asian journal of transfusion science* **3**, 86-94, doi:10.4103/0973-6247.53882 (2009).